PHYSICAL REVIEW A **93**, 023838 (2016)

Quantum acousto-optic transducer for superconducting qubits

Vitaly S. Shumeiko
Chalmers University of Technology, S-412 96 Gothenburg, Sweden

(Received 19 November 2015; revised manuscript received 3 February 2016; published 24 February 2016)

We propose theory for a reversible quantum transducer connecting superconducting qubits and optical photons using acoustic waves in piezoelectrics. The proposed device consists of an integrated acousto-optic resonator that utilizes stimulated Brillouin scattering for phonon-photon conversion and piezoelectric effect for coupling of phonons to qubits. We evaluate the phonon-photon coupling rate and show that the required power of the optical pump as well as the other device parameters providing full and faithful quantum conversion is feasible for implementation with the state-of-the-art integrated acousto-optics.

DOI: 10.1103/PhysRevA.93.023838

I. INTRODUCTION

A network of superconducting qubits interconnected and measured with microwave photons constitutes a c-QED (circuit quantum electrodynamics) architecture of a quantum processor [1]. This architecture demonstrated performance of basic quantum algorithms with up to nine qubits on a chip [2–5]; the number of qubits is expected to further increase. However, the microwave photons are not suitable for long-distance quantum communication; the optical channels are required in order to connect remote qubit clusters [6,7]. Development of microwave to optic quantum interfaces is a vital step towards large scale quantum networks. Also, the transferring to the optical domain of complex nonclassical photonic states produced by c-QED technology might be attractive for quantum metrology [8].

The problem of interfacing the c-QED network and optical photons is challenging. It has been extensively discussed theoretically [9], and a number of solutions involving nonlinear optomechanical interfaces have been proposed [7,10–12] and experimentally tested [13,14].

In a parallel development, a strong piezoelectric coupling of a superconducting qubit to propagating surface acoustic waves (SAWs) was experimentally demonstrated [15,16], the coupling rate being comparable to the one in the c-QED devices. In another experiment [17] a SAW resonator demonstrated a high-quality factor, $Q \sim 10^5$, comparable to the microwave resonators. These experiments suggest a possibility of using GHz-frequency phonons for on-chip quantum communication (circuit quantum acousto-dynamics, c-QAD) [18,19]. An attractive feature of c-QAD architecture is a possibility of efficient coupling of phonons to optical photons, thus providing means for long-distance quantum communication.

In this paper we propose and theoretically investigate a quantum acousto-optic transducer that utilizes the mechanism of stimulated Brillouin scattering (SBS) [20] as a tool for reversible phonon-photon conversion.

SBS is a fundamental physical effect of inelastic scattering of light by acoustic waves in the presence of a strong resonant optical field [21]. SBS is observed in a variety of liquid and solid media, and widely used in acousto-optic devices [22–24]. Under SBS the wave vectors of the resonant optical and acoustic modes have comparable values, which allows for efficient conversion of telecom optical photons and acoustic phonons in the GHz-frequency range compatible with the c-QAD technology.

The questions we raise and answer in this paper are (i) how strong is the phonon-photon coupling provided by SBS, and (ii) can full phonon-photon conversion be achieved with realistic intensity of an optical pump?

Stimulation of acousto-optic interaction by a strong resonant field under SBS can be understood as a peculiar hybrid form of a nondegenerate parametric resonance, which couples physically different fields. Similar to purely electromagnetic nondegenerate parametric resonance in c-QED cavities [25–28], SBS appears as either amplification of optical and acoustic modes or mode hybridization and Rabi oscillation [29,30]. At cryogenic temperatures relevant for operation of superconducting qubits, the Rabi oscillation regime maintains full coherence because of small acoustic attenuation. This regime is proposed for the quantum acousto-optic conversion.

The physical interaction underlying Brillouin scattering is a nonlinear photo-elastic effect—a change of the dielectric constant of the resonator material under elastic deformation. This is a common effect for all materials, resulting in many cases in dominant optical nonlinearity [21]. In resonators, the variation of the dielectric constant produces an effect similar to the optomechanical effect of displacement of cavity boundaries [31,32]. Furthermore, a reciprocal to the photoelastic effect is a force exerted by the gradient of the light energy on the elastic medium. Thus the photoelastic effect can be understood as a distributed bulk analog of the physically similar boundary effect in optomechanics.

The purpose of this paper is to formulate a quantum theory of SBS in an integrated acousto-optic resonator and identify conditions for the full reversible phonon-photon conversion.

II. ACOUSTO-OPTIC RESONATOR

The envisioned device is illustrated in Fig. 1. The device in Fig. 1(a) is an extension of the setup of the transmon-SAW experiment [16]. It consists of a high-quality SAW resonator defined on a surface of a piezoelectric crystal by Bragg mirrors. The acoustic signal is excited by a SAW interdigital transducer (IDT) that simultaneously serves as a capacitance for the transmon qubit and is connected to a microwave line. The SAW resonator is integrated with a high-quality optical resonator consisting of a one-dimensional (1D) waveguide loop defined on the surface of the piezoelectric. The optical

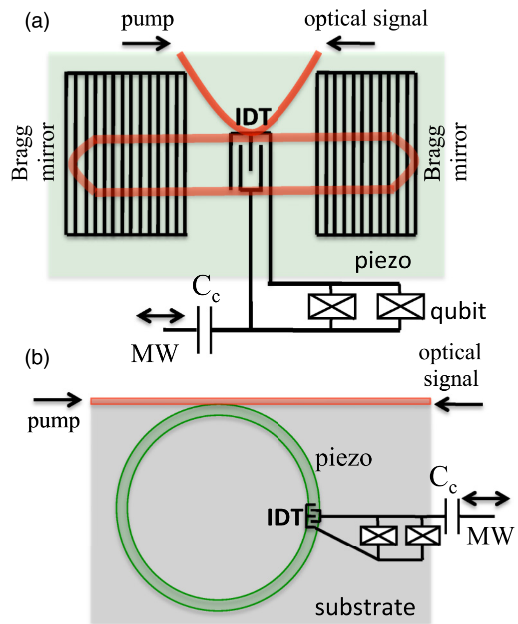

FIG. 1. Acousto-optic transducer. (a) SAW resonator confined by the Bragg mirrors and integrated with the optical resonator (red line) defined at the surface of the piezoelectric and evanescently coupled to a fiber; the transmon qubit capacitor acts as IDT that couples the microwave field to the SAW; C_c is a coupling capacitor to the external microwave line (MW) [16,17]. (b) Integrated SAW-optical ring resonator made with a piezoelectric film [33].

field is injected into and extracted from the resonator by evanescent coupling to a fiber. The optical and acoustic waves coexist in this integrated resonator and interact due to the SBS mechanism. In Fig. 1(b) an integrated acousto-optic resonator with the ring geometry is shown, inspired by the design of existing optomechanical devices [33]. The transducer can also be realized with optomechanical crystals [34] fabricated with piezoelectric materials [13,35].

A. Classical theory of SBS

Within the classical theory of SBS [21,36,37], the photoelastic interaction is introduced through variation of the dielectric constant $\epsilon_{\alpha\beta}$ under elastic deformation $u_{\delta,\gamma}$, $\delta\epsilon_{\alpha\beta} = \gamma_{\alpha\beta\gamma\delta}u_{\delta,\gamma}$, and the interaction strength is quantified with the photo-elastic coefficient tensor $\gamma_{\alpha\beta\gamma\delta}$ [indices denote spatial coordinates (x,y,z), the index after the coma indicates differentiation over the respective variable, and convention is used for summation over repeated indices].

The equations of classical theory of SBS extended to piezoelectric materials read

$$\ddot{D}_\alpha + c^2\,(\mathrm{rotrot\,E})_\alpha = 0, \quad D_{\alpha,\alpha} = 0, \tag{1}$$

$$\rho\ddot{u}_\gamma = c_{\alpha\beta\gamma\delta}u_{\alpha,\beta\delta} + e_{\alpha\beta\gamma}E_{\alpha,\beta} - \frac{\gamma_{\alpha\beta\gamma\delta}}{8\pi}(E_\alpha E_\beta)_{,\delta}, \tag{2}$$

$$D_\alpha = \epsilon_{\alpha\beta}E_\beta - 4\pi e_{\alpha\beta\gamma}u_{\beta,\gamma} + \gamma_{\alpha\beta\gamma\delta}\,E_\beta u_{\gamma,\delta}, \tag{3}$$

where $e_{\alpha\beta\gamma}$ is a piezoelectric tensor [38], ρ is a mass density, and $c_{\alpha\beta\gamma\delta}$ is a stiffness tensor. These equations follow from a general Lagrangian for the acousto-optic system [39],

$$\mathcal{L} = \frac{1}{2}\int dV\Big[\frac{E^2 - H^2}{4\pi} + \varphi\,P_{\alpha,\alpha} + \frac{1}{c}A_\alpha\dot{P}_\alpha + \dot{u}_\alpha^2 - c_{\alpha\beta\gamma\delta}u_{\alpha,\beta}u_{\gamma,\delta}\Big], \tag{4}$$

by computing variations over electromagnetic potentials, A_α and φ, and displacement u_α. Here $P_\alpha = \chi_{\alpha\beta}E_\beta - 2e_{\alpha\beta\gamma}u_{\beta,\gamma} + (1/4\pi)\gamma_{\alpha\beta\gamma\delta}E_\beta u_{\gamma,\delta}$ is a macroscopic polarization vector and $\chi_{\alpha\beta}$ is an electric susceptibility. The details of the derivation are presented in the Appendix.

The last nonlinear term in the elasticity equation (2) describes the pressure exerted by the electromagnetic field on the elastic medium. This nonlinear term generates a mixture of optical modes, which may propagate with the speed of sound allowing for strong resonant interaction between acoustic and optical fields. This interaction is supported by resonant scattering of light in Eq. (1) by spatiotemporal grating formed by the sound. This is the classical wave picture of the Brillouin scattering.

Dynamics of the acousto-optic system, Eqs. (1)–(3), consists of two different time scales associated with different propagation velocities of the light and the sound. These time scales are resolved by separating the fast transverse (optical) component of the electric field, $E^t_\alpha = -(1/c)\dot{A}_\alpha$, $E^t_{\alpha,\alpha} = 0$,

$$\epsilon_{\alpha\beta}\ddot{A}_\beta - c^2\,\Delta A_\alpha + \gamma_{\alpha\beta\gamma\delta}\,\partial_t(\dot{A}_\beta u_{\gamma,\delta}) = 0, \tag{5}$$

and the slow longitudinal piezoelectric component, $E^l_\alpha = -\varphi_{,\alpha}$, rot $E^l_\alpha = 0$, coupled to the elastic field:

$$\begin{aligned}\rho\ddot{u}_\gamma - c_{\alpha\beta\gamma\delta}u_{\alpha,\beta\delta} - e_{\alpha\beta\gamma}\varphi_{,\alpha\beta} + \frac{\gamma_{\alpha\beta\gamma\delta}}{8\pi c^2}\overline{(\dot{A}_\alpha\dot{A}_\beta)}_{,\delta} &= 0,\\ \epsilon_{\alpha\beta}\,\varphi_{,\alpha\beta} + 4\pi\,e_{\alpha\beta\gamma}u_{\beta,\gamma\alpha} &= 0,\end{aligned} \tag{6}$$

where the bar indicates averaging over fast optical oscillation. In Eq. (6) a nonlinear term containing small piezoelectric potential was omitted (for the details of derivation see the Appendix). The shortened equations (5) and (6) are associated with the Lagrangian, which we divide into the free field part, $\mathcal{L}_0$, and the photoelastic interaction part, $\mathcal{L}_{\rm int}$:

$$\begin{aligned}\mathcal{L} &= \mathcal{L}_0 + \mathcal{L}_{\rm int},\\ \mathcal{L}_0 &= \frac{1}{2}\int dV\,\Big\{\frac{1}{4\pi c^2}\epsilon_{\alpha\beta}\dot{A}_\alpha\dot{A}_\beta - \frac{1}{4\pi}A_{\alpha,\beta}A_{\alpha,\beta} + \rho\dot{u}_\alpha^2\\ &\quad - c_{\alpha\beta\gamma\delta}\,u_{\alpha,\beta}u_{\gamma,\delta} + 2e_{\alpha\beta\gamma}\,u_{\beta,\gamma}\varphi_{,\alpha} + \frac{1}{4\pi}\epsilon_{\alpha\beta}\,\varphi_{,\alpha}\varphi_{,\beta}\Big\},\\ \mathcal{L}_{\rm int} &= \frac{1}{2}\int dV\,\frac{1}{4\pi c^2}\gamma_{\alpha\beta\gamma\delta}\,u_{\gamma,\delta}\dot{A}_\alpha\dot{A}_\beta.\end{aligned} \tag{7}$$

B. Ring resonator

The SBS equations are formulated for a boundless continuous medium. To consider fields confined in a resonator, we focus for certainty on the ring resonator geometry of Fig. 1(b), with the ring circumference much larger than the wavelength, $L \gg \lambda$. The eigenmodes of such a resonator can be approximated with the ones of a 1D waveguide with the periodic boundary condition along the x direction. We expand the fields over the eigenmodes of the noninteracting resonator:

$$A_\alpha(r,t) = (1/\sqrt{L}) \sum_{k,n} A_n(k,t) e^{ikx} \psi_\alpha^n(r_\perp,k), \tag{8}$$

$$u_\alpha(r,t) = (1/\sqrt{L}) \sum_{q,m} u_m(q,t) e^{iqx}\, \phi_\alpha^m(r_\perp,q), \tag{9}$$

were the normalized eigenfunctions, $\psi_\alpha^n(r_\perp,k)$ and $\phi_\alpha^m(r_\perp,q)$, describe the transverse confinement of the respective fields, indices n,m count the transverse eigenmodes.

The exact form of the transverse eigenfunctions is dictated by particular geometry of the wave guide. Computing these functions analytically is particularly difficult for the acoustic modes, the difficulty results from the material anisotropy that mixes field components even in the bulk, but is further complicated by the boundary conditionsn [38,39]. Some analytical solutions are only available for isotropic and nonpiezoelectric wave guides [40]. For our purposes, however, no explicit form of the eigenfunctions is needed but rather their general properties are needed.

Restricting ourselves for simplicity to optically isotropic materials, the optical eigenfunctions are found from the equation

$$[\Delta_\perp - k^2]\psi_\alpha^n(r_\perp,k) = -\left[\epsilon\omega_n^2(k)/c^2\right]\psi_\alpha^n(r_\perp,k), \tag{10}$$

complemented with appropriate boundary conditions; $\omega_n(k)$ is the frequency of the nth mode.

The equation for the acoustic eigenmodes is derived by eliminating piezoelectric potential using the second equation in Eq. (6), yielding

$$\hat{\mathcal{D}}_{\alpha\gamma}[q]\phi_\gamma^m(r_\perp,q) = -\rho\,\Omega_m^2(q)\phi_\alpha^m(r_\perp,q), \tag{11}$$

where

$$\hat{\mathcal{D}}_{\alpha\gamma}[q] = \left[c_{\alpha\beta\gamma\delta} - \frac{4\pi e_{\lambda\mu\alpha}e_{\beta\gamma\delta}}{\epsilon}\partial_\lambda\partial_\mu(\Delta_\perp - q^2)^{-1}\right]\partial_\beta\partial_\delta$$

is a nonlocal operator with $\partial_x = iq$, and $\Omega_m(q)$ is the frequency of the mth transverse mode. The solutions are generally complex and obey the symmetry relation, $\phi_\alpha^m(r_\perp,-q) = [\phi_\alpha^m(r_\perp,q)]^*$.

Within the eigenmode representation, the free field part of the Lagrangian in Eq. (7) has the form

$$\mathcal{L}_0 = \frac{\epsilon}{8\pi c^2}\sum_{k,n}\left\{\dot{A}_n(k)\dot{A}_n(-k) - \omega_n^2(k)A_n(k)A_n(-k)\right\}$$
$$+ \frac{\rho}{2}\sum_{n,q}\left\{\dot{u}_n(q)\dot{u}_n(-q) - \Omega_n^2(q)u_n(q)u_n(-q)\right\}, \tag{12}$$

while the Lagrangian of the photoelastic interaction reads

$$\mathcal{L}_{\rm int} = \frac{1}{8\pi c^2}\sum_{\substack{nn'm\\kk'q}}\mathcal{M}_{nn'm}^{kk'q}\,\dot{A}_n(k)\dot{A}_{n'}(k')u_m(q), \tag{13}$$

$$\mathcal{M}_{nn'm}^{kk'q} = \gamma_{\alpha\beta\gamma\delta}\int\frac{dV}{\sqrt{L^3}}\,\psi_\alpha^n(r_\perp,k)\psi_\beta^{n'}(r_\perp,k')$$
$$\times e^{i(k+k')x}\left(\phi_\gamma^m(r_\perp,q)e^{iqx}\right)_{,\delta}. \tag{14}$$

The major contribution to the interaction is given by the resonant wave triads selected by the resonance conditions, $\omega_{n'}(k') - \omega_n(k) = \Omega_m(q)$ and $k' - k = q$. These equations define the scattering geometry with the optical modes propagating in opposite directions and having wave vectors, $k' \approx -k = (q/2)[1 + O(\Omega/\omega)]$, $\Omega \ll \omega$; the acoustic mode propagates along the direction of the optical mode with larger frequency. Truncated to the resonant subspace, the Lagrangian (13) reduces to the sum over resonant triads, each contribution having the form of the resonant three-wave interaction:

$$\mathcal{L}_{\rm int} \sim A_n(k)A_{n'}^*(k')u_m(q) + A_n^*(k)A_{n'}(k')u_m^*(q). \tag{15}$$

This interaction is generally known in theory of nonlinear waves [41], and it describes scattering between two optical modes with emission and absorption of the acoustic mode. We note that the frequencies of the optical modes in Eq. (15) obey the inequality $\omega_{n'k'} > \omega_{nk}$.

C. SBS in the quantum regime

To proceed with the quantum description of SBS, we consider one of the optical modes to have much larger amplitude than the other and treat this pumping mode as a classical coherent state characterized by the number N_p of pumping photons, $A_p \propto \sqrt{N}_p e^{-i\omega_p t}$. Then we apply the quantization procedure to weak optical and acoustic modes.

The quantization is performed, first, by deriving the Hamiltonian in the mode representation using Eqs. (12) and (13); then complex dimensionless quadratures are introduced via canonical transformation,

$$\begin{aligned} A_n(k) &= \sqrt{2\pi\hbar c^2/\epsilon\omega_n(k)}\,(a_{nk} + a_{n(-k)}^*),\\ u_m(q) &= \sqrt{\hbar/2\rho\Omega_m(q)}(b_{mq} + b_{m(-q)}^*), \end{aligned} \tag{16}$$

and the canonical commutation relations are imposed on these quadratures, $[a_{nk},a_{nk}^\dagger] = 1$, and $[b_{mq},b_{mq}^\dagger] = 1$.

Selection of the pumping mode leads to the two different types of quantum Hamiltonians depending on whether the frequency of the pumping mode is smaller or larger than the frequency of the optical signal mode. In the first case, $\omega_p = \omega_s - \Omega$ [pumping mode is $A_n(k)$ in Eq. (15)], the scattering occurs with absorption of the phonon into a blue-shifted (anti-Stokes) sideband. This process results in the coherent phonon-photon conversion and is described with the beam splitter type Hamiltonian:

$$\mathcal{H}_{\rm SBS} = -\hbar\sqrt{N}_p(g_0e^{-i\omega_p t}\,a^\dagger b + g_0^* e^{i\omega_p t}\,ab^\dagger). \tag{17}$$

In the second case, $\omega_p = \omega_s + \Omega$ [mode $A_{n'}(k')$ is chosen as the pump], the scattering occurs with emission of phonon to a red-shifted (Stokes) sideband. In this case, the SBS Hamiltonian takes the form of a parametric amplifier,

$$\mathcal{H}_{\rm SBS} = -\hbar\sqrt{N}_p(g_0e^{-i\omega_p t}\,a^\dagger b^\dagger + g_0^* e^{-i\omega_p t}\,ab), \tag{18}$$

and describes the amplification and two-mode squeezing of the optical and acoustic modes [42].

In both cases, the acousto-optic coupling is given by the vacuum phonon-photon coupling rate, g_0,

$$g_0 = \mathcal{M}\sqrt{\frac{\hbar\omega_p\omega_s\Omega}{32\epsilon^2\rho s^2}}, \tag{19}$$

enhanced by the pumping field. Here $\mathcal{M}$ is the overlap integral in Eq. (14) truncated to the resonant subspace,

$$\mathcal{M} = \frac{\gamma_{\alpha\beta\gamma\delta}}{\sqrt{L}} \int dV_\perp \psi^p_\alpha(r_\perp,q/2)\psi_\beta(r_\perp,q/2) \times (\partial_\delta/q + i\delta_{\delta x})\phi_\gamma(r_\perp,q), \tag{20}$$

where superscript p indicates the pumping mode. For an optimal design of the resonator, $\mathcal{M}$ is estimated,

$$\mathcal{M} \sim \gamma/\sqrt{V}, \tag{21}$$

where γ is a representative value of the photoelastic tensor, and V is the resonator volume.

For piezoelectric materials with relatively large photoelastic interaction, such as $LiNbO_3$ and GaAs, the vacuum coupling rate is estimated, $g_0 \sim 1.7\ \mathrm{MHz}/\sqrt{V[\mu^3]}$ ($LiNbO_3$), and $g_0 > 6\ \mathrm{MHz}/\sqrt{V[\mu^3]}$ (GaAs), while for AlN it is below 100 KHz due to a small photoelastic constant.

Our estimate for the vacuum coupling rate is solely based on the consideration of the photoelastic interaction. In literature an additional mechanism of acousto-optic coupling is considered stemming from the displacement of resonator boundaries [34,43,44]. Although this effect is described with a similar nonlinear three-wave interaction to the one in Eq. (15) [31,32], the underlying physics is different in both cases: The photoelastic effect affects the light velocity, while the boundary displacement changes geometric quantization of the cavity modes. Furthermore the boundary effect in its generic form [31,45] assumes a sharp stepwise boundary the displacement of which results in a large change of the dielectric constant that cannot be described with the photoelastic effect. However, in practice the boundaries of integrated solid-state waveguides are smooth on the scale of the zero-point acoustic displacement, hence variation of the dielectric constant under elastic deformation is small. This justifies the photoelastic approximation not only in the bulk but also at the boundary, while the optomechanical boundary effect does not play a separate role.

D. Conversion efficiency

To evaluate the fidelity and efficiency of the phonon-photon conversion, we assume the qubit is well detuned from the acoustic resonance and consider the transducer as a four-port device having optical and microwave input and output ports. For the optical ports, the input-output relation has conventional form [46], $a_{\rm out} = a_{\rm in} - i\sqrt{2\kappa_0}\,a$, where κ_0 is a coupling rate to the optical fiber. Considering the microwave ports, we introduce the microwave field operators in the external transmission line, $c_{\rm in}$ and $c_{\rm out}$, and write the input-output relation taking advantage of the linear piezoelectric coupling of microwave and acoustic fields, $c_{\rm out} = c_{\rm in} - i\sqrt{2\Gamma_0}\,b$, where Γ_0 includes the coupling rates of the IDT and the capacitive connection, C_c, to the transmission line, Fig. 1.

The intracavity field operators satisfy the Langevin equations, associated with Hamiltonian (17), which have the form in the interaction representation

$$\begin{aligned} i\dot{a} + (\delta\omega + i\kappa)a + g_0\sqrt{N_p}b &= \sqrt{2\kappa_0}\,a_{\rm in},\\ i\dot{b} + (\delta\Omega + i\Gamma)b + g_0^*\sqrt{N_p}a &= \sqrt{2\Gamma_0}\,c_{\rm in}. \end{aligned} \tag{22}$$

Here we introduced detunings of the input optical signal, $\delta\omega$, and acoustic signal, $\delta\Omega$, from the respective resonances, that satisfy the relation $\delta\omega - \delta\Omega = 2\delta$, with 2δ referring to detuning of the pump, $\omega_p = \omega_s - \Omega + 2\delta$; κ and Γ denote total optical and acoustic damping rates, respectively.

Solving these equations and substituting into the input-output relations, we compute the scattering matrix and evaluate the transmission and reflection amplitudes:

$$\begin{aligned} S_{11} &= 1 - 2i\kappa_0(\delta\Omega + i\Gamma)/D,\\ S_{22} &= 1 - 2i\Gamma_0(\delta\omega + i\kappa)/D,\\ S_{12} &= -2ig_0\sqrt{N_p\kappa_0\Gamma_0}/D, \end{aligned} \tag{23}$$

where $D = (\delta\omega + i\kappa)(\delta\Omega + i\Gamma) - |g_0|^2 N_p$.

In the limit of negligibly small internal losses, $\kappa - \kappa_0 \ll \kappa_0$, and $\Gamma - \Gamma_0 \ll \Gamma_0$, the scattering matrix acquires a unitary form with $|S_{11}| = |S_{22}|$, and $|S_{12}| = |S_{21}| = 1 - |S_{11}|^2$, thus providing reversibility of phonon-photon conversion.

Furthermore, a full conversion indicated by absence of the reflection, $|S_{11}| = |S_{22}| = 0$, is achieved for

$$|g_0|^2 N_p \geqslant \kappa_0\Gamma_0, \tag{24}$$

the equality occurring at the exact resonance, $\delta\omega = \delta\Omega = 0$, as illustrated in Fig. 2. This equation defines the minimum pump strength required for the full phonon-photon conversion. For realistic Q-factor values, $Q_{\rm opt} = \omega_s/\kappa \sim 10^5$ and $Q_{ac} = \Omega/\Gamma \sim 10^4$, the corresponding pump photon density is estimated, $N_p/V \sim 10^4\ \mathrm{photons}/\mu^3$, for $LiNbO_3$. It is interesting that this minimum value coincides with the threshold of parametric oscillation in the Stokes scattering channel, where the amplified phonon-photon vacuum noise reaches its maximum value [28,47]. Above the threshold, the full conversion can be achieved for finite detunings, $\delta\omega = \kappa_0(|g|^2/\kappa_0\Gamma_0 - 1)^{1/2}$, and $\delta\Omega = (\Gamma_0/\kappa_0)\delta\omega$.

For the purpose of faithful single quantum phonon-photon conversion, the Stokes scattering is an undesirable process, since it generates spurious phonon-photon pairs out of the vacuum fluctuations. The Stokes scattering can be suppressed by making the Stokes sideband frequency well detuned from the cavity resonance. This imposes a constraint on

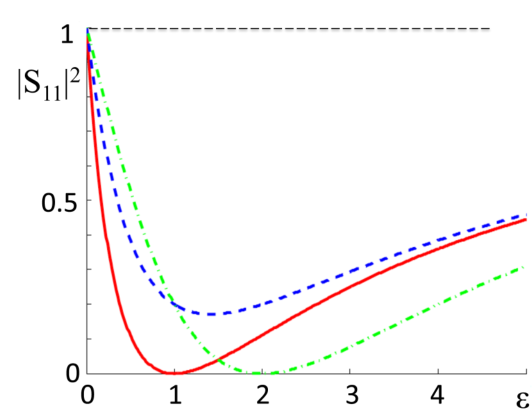

FIG. 2. Conversion efficiency as a function of normalized pumping strength, $\varepsilon = |g_0|^2 N_p/\kappa_0\Gamma_0$, for different pump and signal detunings; internal losses are neglected. Solid (red) line: exact resonance, $\delta = \delta\omega_s = \delta\Omega = 0$. Dash-dotted (green) line: $\delta\omega_s = \kappa_0$, $\delta\Omega = \Gamma_0$, $\delta = (\kappa_0 - \Gamma_0)/2$. Dashed (blue) line: $\delta = 0$, $\delta\Omega = \delta\omega_s = \Gamma_0$.

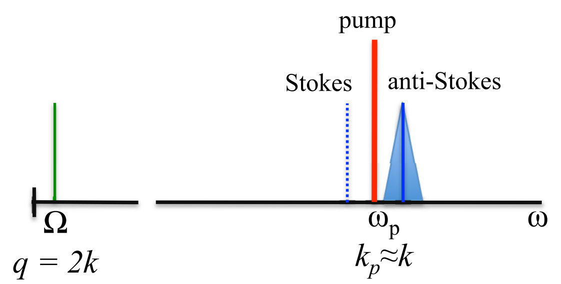

FIG. 3. Frequency diagram of the SBS: the scattering occurs into two sidebands symmetrically shifted from the pump frequency by $\pm\Omega$; the blue triangle indicates broadening of the cavity resonance, $\kappa_0 < 2\Omega$.

the resonance width, $\kappa < 2\Omega$, corresponding to the resolved sideband regime, as illustrated in Fig. 3. Accordingly the optical Q factor has a lower bound, $Q_{\rm opt} > \omega_s/2\Omega \sim 2\times 10^4$. Additional possibility for suppressing the Stokes scattering exists in the ring resonator of Fig. 1(b): taking advantage of the asymmetry of the Brillouin scattering, one may implement asymmetric IDT to selectively emit and absorb acoustic waves moving in the direction only supporting the anti-Stokes scattering.

III. PRACTICAL IMPLEMENTATION

The transducer performance—fidelity and efficiency of the phonon-photon conversion—depends on a number of material and device parameters. The most important limitation on these parameters is imposed by the requirement of minimum heating effect of the pump losses, which is damaging for a fragile cryogenic environment of c-QED devices. This implies minimization of the pump power, Eq. (24), required for the full conversion. This is achieved by reducing external optical and acoustic losses, and choosing materials with large phonon-photon vacuum coupling rate. However, the engineered external losses cannot be made arbitrarily small—they must significantly exceed the internal losses in order to maintain the unitarity of the conversion, Eq. (23). For the optical internal damping at the level of $\sim 0.1\,\kappa_0 \sim 1$ GHz, the estimated dissipated power density within the resonator would be $\sim 1\ \mu\mathrm{W}/\mu^3$ (for $LiNbO_3$).

Furthermore, to maximally reduce the heating effect, it is desirable to confine the losses to the interaction volume within the resonator, while keeping low pump power in the feeding fiber. To achieve this one needs to engineer additional narrow resonance at the pump frequency; then estimated pump power would be within the range of 10 μW. The resonator with two tightly spaced and resolved optical resonances could be realized using the method of coupled cavities [48].

The value of the vacuum coupling rate, Eq. (19), is essentially defined by the photoelastic coefficient and the resonator volume. The photoelastic interaction is quantified in literature with the Pockel coefficient p, related to our coefficient, $\gamma = pn^4$, where n is the refractive index. For piezoelectric materials of interest, the largest Pockel coefficients vary from $p = 0.02$, in AlN, to $p > 0.16$, in GaAs and $LiNbO_3$. Correspondingly, the variation of γ is in the range 0.3–20. Since the minimum pump power is proportional to the squared photoelastic coefficient, the required pump power may differ by up to three orders of magnitude depending on the choice of material.

The cavity volume is to be reduced to maximize the vacuum coupling rate. In this respect, the optomechanical crystal resonators [13,34,35] seem to provide an ultimate solution, having the volume of a few cubic wavelengths. The integrated ring resonator depicted in Fig. 1(b) is more favorable compared to the planar SAW device in Fig. 1(a) since it may have small transverse dimensions comparable to the wavelength, while the width of the planar SAW resonator is of the order of tens wavelengths (although this can be reduced by using focusing mirrors). Furthermore, the planar resonator has a large length, up to 1000 wavelengths [17], due to weak localization effect of metallic fingers of the Bragg mirrors that induce very small modulation of the SAW velocity [49].

IV. CONCLUSION

We proposed and performed theoretical analysis of a reversible quantum transducer for coupling microwave and optical photons. The transducer employs acoustic phonons in the GHz-frequency range as an intermediate agent and consists of an integrated acousto-optic cavity fabricated with piezoelectric material. The phonon-optical photon conversion is provided by the mechanism of stimulated Brillouin scattering (SBS), while the phonon-microwave photon conversion is due to the piezoelectric effect. We find that the SBS induced vacuum coupling rate is in the range of a few MHz per μ^3 cavity volume, and the full phonon-photon conversion can be achieved at pump power of tens of μW. Our analysis of the material and device parameters that would provide full and faithful quantum phonon-photon conversion is feasible for implementation with the state-of-the-art integrated acousto-optics.

ACKNOWLEDGMENTS

The author is thankful for useful discussions to Magnus Karlsson, Martin Gustafsson, Per Delsing, Thomas Aref, Peter Leek, Victor Torres, and Göran Wendin. Support from the EU FP-7 IP SCALEQIT is gratefully acknowledged.

APPENDIX: DERIVATION OF CLASSICAL SBS EQUATIONS

The starting point is the macroscopic action for an acousto-optic medium consisting of electromagnetic and elastic parts:

$$S = \int dt\ \mathcal{L},$$
$$\mathcal{L} = \frac{1}{2}\int dV\left(\frac{E^2 - H^2}{4\pi} + \varphi P_{\alpha,\alpha} + \frac{1}{c}A_\alpha \dot{P}_\alpha + \rho\dot{u}^2 - c_{\alpha\beta\gamma\delta}u_{\alpha,\beta}u_{\gamma,\delta}\right). \tag{A1}$$

Macroscopic polarization, $P_\alpha = \chi_{\alpha\beta}E_\beta - 2e_{\alpha\beta\gamma}u_{\beta,\gamma} + (1/4\pi)\gamma_{\alpha\beta\gamma\delta}E_\beta u_{\gamma,\beta}$, contains piezoelectric and photoelastic interaction terms, $E_\alpha = -\varphi_{,\alpha} - (1/c)\dot{A}_\alpha$, $H_\alpha = (\mathrm{rot}\, A)_\alpha$;

magnetic effects are not included in this calculation. The tensor coefficients entering the Lagrangian possess symmetries:

$$e_{\alpha\beta\gamma} = e_{\alpha\gamma\beta}, \quad \gamma_{\alpha\beta\gamma\delta} = \gamma_{\gamma\delta\alpha\beta} = \gamma_{\beta\alpha\gamma\delta} = \gamma_{\alpha\beta\delta\gamma},$$
$$c_{\alpha\beta\gamma\delta} = c_{\gamma\delta\alpha\beta} = c_{\beta\alpha\gamma\delta} = c_{\alpha\beta\delta\gamma}. \tag{A2}$$

Variation of the electromagnetic part of the Lagrangian is conveniently done in two steps. First we compute variation over variable E_α, that explicitly enters the Lagrangian:

$$\delta\mathcal{L}_E = \frac{1}{4\pi}\int dV[(\epsilon_{\alpha\beta} - 2\pi\,\chi_{\alpha\beta} + \gamma_{\alpha\beta\gamma\delta}u_{\gamma,\delta})E_\beta]\delta E_\alpha,$$
$$\epsilon_{\alpha\beta} = \delta_{\alpha\beta} + 4\pi\,\chi_{\alpha\beta}. \tag{A3}$$

Then we express this variation in the terms of variations of electromagnetic potentials:

$$\delta\mathcal{L}_E = \frac{1}{4\pi}\int dV\left\{\left(\epsilon_{\alpha\beta}\dot{E}_\beta - 2\pi\,\chi_{\alpha\beta}\dot{E}_\beta + \frac{1}{2}\gamma_{\alpha\beta\gamma\delta}\partial_t(u_{\gamma,\delta}E_\beta)\right)\frac{1}{c}\delta A_\alpha + \left(\epsilon_{\alpha\beta}E_{\beta,\alpha} - 2\pi\,\chi_{\alpha\beta}E_{\beta,\alpha} + \frac{1}{2}\gamma_{\alpha\beta\gamma\delta}(u_{\gamma,\delta}E_\beta)_{,\alpha}\right)\delta\varphi\right\}. \tag{A4}$$

The next step is to compute the variation due to explicitly entering Eq. (A1) variables A_α and φ:

$$\delta\mathcal{L}_{A,\varphi} = \frac{1}{4\pi}\int dV\left\{\frac{1}{c}\left(2\pi\,\chi_{\alpha\beta}\dot{E}_\beta - 4\pi\,e_{\alpha\beta\gamma}\dot{u}_{\beta,\gamma} + \frac{1}{2}\gamma_{\alpha\beta\gamma\delta}\,\partial_t(E_\beta u_{\gamma,\delta}) - c(\mathrm{rot}H)_\alpha\right)\delta A_\alpha + \left(2\pi\,\chi_{\alpha\beta}E_{\beta,\alpha} - 4\pi\,e_{\alpha\beta\gamma}u_{\beta,\gamma\alpha} + \frac{1}{2}\gamma_{\alpha\beta\gamma\delta}(E_\beta u_{\gamma,\delta})\right)_{,\alpha}\delta\varphi\right\}. \tag{A5}$$

The total variation of the electromagnetic part of the Lagrangian consists of the sum of these two parts, $\delta\mathcal{L}_{Em} = \delta\mathcal{L}_E + \delta\mathcal{L}_{A,\varphi}$:

$$\delta\mathcal{L}_{Em} = \frac{1}{4\pi}\int dV\left\{\left(\frac{1}{c}\dot{D}_\alpha - (\mathrm{rot\,H})_\alpha\right)\delta A_\alpha + D_{\alpha,\alpha}\delta\varphi\right\}, \tag{A6}$$

conveniently written through the electric displacement defined by the equation

$$D_\alpha = \epsilon_{\alpha\beta}E_\beta - 4\pi\,e_{\alpha\beta\gamma}u_{\beta,\gamma} + \gamma_{\alpha\beta\gamma\delta}\,E_\beta u_{\gamma,\beta}. \tag{A7}$$

Variation of the Lagrangian over elastic displacement yields

$$\delta\mathcal{L}_{El} = \int dV\left\{-\rho\ddot{u}_\gamma + c_{\alpha\beta\gamma\delta}u_{\alpha,\beta\delta} + e_{\alpha\beta\gamma}E_{\alpha,\beta} - \frac{1}{8\pi}\gamma_{\alpha\beta\gamma\delta}(E_\alpha E_\beta)_{,\delta}\right\}\delta u_\gamma. \tag{A8}$$

From Eqs. (A6) and (A8) we extract equations of motion:

$$\dot{D}_\alpha = c\,(\mathrm{rot\,H})_\alpha, \quad c\,(\mathrm{rotE})_\alpha = -\,\dot{H}_\alpha, \quad D_{\alpha,\alpha} = 0, \tag{A9}$$

$$\rho\ddot{u}_\gamma = c_{\alpha\beta\gamma\delta}u_{\alpha,\beta\delta} + e_{\alpha\beta\gamma}E_{\alpha,\beta} - \frac{1}{8\pi}\gamma_{\alpha\beta\gamma\delta}(E_\alpha E_\beta)_{,\delta}, \tag{A10}$$

which are presented in the main text, Eqs. (1)–(3).

Equations of motion can be significantly simplified due to the fact that the optical field has much larger phase velocity than the acoustic field. For comparable wave vectors of both fields this implies that the time variation of the transverse optical field, A_α, is much faster than the time variation of the acoustic field, u_α, and the related longitudinal piezoelectric field, φ. Therefore one may omit small terms in Eq. (A9) proportional to the time derivatives of u_α, and φ, giving

$$\epsilon_{\alpha\beta}\ddot{A}_\beta - \frac{c^2}{\mu}\Delta\,A_\alpha + \gamma_{\alpha\beta\gamma\delta}\,\ddot{A}_\beta u_{\gamma,\delta} = 0. \tag{A11}$$

Averaging over fast temporal oscillation in Eqs. (A7) and (A10) eliminates the linear terms proportional to A_α, but retains the quadratic term essential for the SBS:

$$\rho\ddot{u}_\gamma - c_{\alpha\beta\gamma\delta}u_{\alpha,\beta\delta} + e_{\alpha\beta\gamma}\varphi_{,\alpha\beta} + \frac{1}{8\pi c^2}\gamma_{\alpha\beta\gamma\delta}(\overline{\dot{A}_\alpha\dot{A}_\beta})_{,\delta} + \frac{1}{8\pi}\gamma_{\alpha\beta\gamma\delta}(\varphi_{,\alpha}\varphi_{,\beta})_{,\delta} = 0$$
$$-\,\epsilon_{\alpha\beta}\varphi_{,\beta\alpha} - 4\pi\,e_{\alpha\beta\gamma}u_{\beta,\gamma\alpha} - \gamma_{\alpha\beta\gamma\delta}(\varphi_{,\beta}u_{\gamma,\delta})_{,\alpha} = 0. \tag{A12}$$

Finally, bearing in mind that under SBS only the optical field contains a large amplitude component, while piezoelastic fields are weak, we omit the last nonlinear terms in both lines of Eq. (A12). The resulting equations are presented in the main text, Eqs. (5) and (6).

[1] R. J. Schoelkopf and S. M. Girvin, Nature (London) **451**, 664 (2008).

[2] L. Steffen, A. Fedorov, M. Oppliger, Y. Salathe, P. Kurpiers, M. Baur, G. Puebla-Hellmann, C. Eichler, and A. Wallraff, Nature (London) **500**, 319 (2013).

[3] D. Riste, M. Dukalski, C. A. Watson, G. de Lange, M. J. Tiggelman, Ya. M. Blanter, K. W. Lehnert, R. N. Schouten, and L. DiCarlo, Nature (London) **502**, 350 (2013).

[4] S. Shankar, M. Hatridge, Z. Leghtas, K. M. Sliwa, A. Narla, U. Vool, S. M. Girvin, L. Frunzio, M. Mirrahimi, and M. H. Devoret, Nature (London) **504**, 419 (2013).

[5] J. Kelly, R. Barends, A. G. Fowler, A. Megrant, E. Jeffrey, T. C. White, D. Sank, J. Y. Mutus, B. Campbell, Yu Chen, Z. Chen, B. Chiaro, A. Dunsworth, I.-C. Hoi, C. Neill, P. J. J. O'Malley, C. Quintana, P. Roushan, A. Vainsencher, J. Wenner, A. N. Cleland, and J. M. Martinia, Nature (London) **519**, 66 (2015).

[6] H. J. Kimble, Nature (London) **453**, 1023 (2008).

[7] K. Stannigel, P. Rabl, A. S. Sorensen, P. Zoller, and M. D. Lukin, Phys. Rev. Lett. **105**, 220501 (2010).

[8] V. Giovannetti, S. Lloyd, and L. Maccone, Phys. Rev. Lett. **96**, 010401 (2006).

[9] M. Wallquist, K. Hammerer, P. Rabl, M. Lukin, and P. Zoller, Phys. Scr. **T137**, 014001 (2009).

[10] A. H. Safavi-Naeini and O. Painter, New J. Phys. **13**, 013017 (2011).

[11] Sh. Barzanjeh, D. Vitali, P. Tombesi, and G. J. Milburn, Phys. Rev. A **84**, 042342 (2011).

[12] Sh. Barzanjeh, M. Abdi, G. J. Milburn, P. Tombesi, and D. Vitali, Phys. Rev. Lett. **109**, 130503 (2012).

[13] J. Bochmann, A. Vainsencher, D. D. Awschalom, and A. N. Cleland, Nature Phys. **9**, 712 (2013).

[14] R. W. Andrews, R. W. Peterson, T. P. Purdy, K. Cicak, R. W. Simmonds, C. A. Regal, and K. W. Lehnert, Nature Phys. **10**, 321 (2014).

[15] M. V. Gustafsson, P. V. Santos, G. Johansson, and P. Delsing, Nature Phys. **8**, 338 (2012).

[16] M. V. Gustafsson, Th. Aref, A. Frisk Kockum, M. K. Ekstrm, G. Johansson, and P. Delsing, Science **346**, 207 (2014).

[17] E. B. Magnusson, B. H. Williams, R. Manenti, M.-S. Nam, A. Nersisyan, M. J. Peterer, A. Ardavan, and P. J. Leek, Appl. Phys. Lett. **106**, 063509 (2015).

[18] S. J. M Habraken, K. Stannigel, M. D. Lukin, P. Zoller, and P. Rabl, New J. Phys. **14**, 115004 (2012).

[19] M. J. A. Schuetz, E. M. Kessler, G. Giedke, L. M. K. Vandersypen, M. D. Lukin, and J. I. Cirac, Phys. Rev. X **5**, 031031 (2015).

[20] R. Y. Chiao, C. H. Townes, and B. P. Stoicheff, Phys. Rev. Lett. **12**, 592 (1964).

[21] R. W. Boyd, *Nonlinear Optics* (Academic, New York, 2008).

[22] E. P. Ippen and R. H. Stolen, Appl. Phys. Lett. **21**, 539 (1972).

[23] J. Beugnot, S. Lebrun, G. Pauliat, H. Maillotte, V. Laude, and T. Sylvestre, Nature Comm. **5**, 5242 (2014).

[24] G. Bahl and T. Carmon, in *Cavity Optomechanics*, edited by M. Aspelmeyer, T. J. Kippenberg, and F. Marquardt (Springer, New York, 2014), Chap. 8.

[25] E. Flurin, N. Roch, F. Mallet, M. H. Devoret, and B. Huard, Phys. Rev. Lett. **109**, 183901 (2012).

[26] E. Zakka-Bajjani, F. Nguyen, M. Lee, L. R. Vale, R. W. Simmonds, and J. Aumentado, Nature Phys. **7**, 599 (2011).

[27] B. Abdo, K. Sliwa, F. Schackert, N. Bergeal, M. Hatridge, L. Frunzio, A. D. Stone, and M. H. Devoret, Phys. Rev. Lett. **110**, 173902 (2013).

[28] M. Simoen, C. W. S. Chang, P. Krantz, Jonas Bylander, W. Wustmann, V. Shumeiko, P. Delsing, and C. M. Wilson, J. Appl. Phys. **118**, 154501 (2015).

[29] Chap. Galland, N. Sangouard, N. Piro, N. Gisin, and T. J. Kippenberg, Phys. Rev. Lett. **112**, 143602 (2014).

[30] F. Lecocq, J. D. Teufel, J. Aumentado, and R. W. Simmonds, Nature Phys. **11**, 635 (2015).

[31] C. K. Law, Phys. Rev. A **51**, 2537 (1995).

[32] A. A. Clerk and F. Marquardt, in *Cavity Optomechanics*, edited by M. Aspelmeyer, T. J. Kippenberg, and F. Marquardt (Springer, New York, 2014), Chap. 2, pp. 5–24.

[33] Chi Xiong, Xiankai Sun, King Y. Fong, and Hong X. Tang, Appl. Phys. Lett. **100**, 171111 (2012).

[34] A. H. Safavi-Naeini and O. Painter, in *Cavity Optomechanics*, edited by M. Aspelmeyer, T. J. Kippenberg, and F. Marquardt (Springer, New York, 2014), Chap. 10, pp. 195–232.

[35] K. C. Balram, M. Davanco, J.-D. Song, and K. Srinivasan, arXiv:1508.01486 [physics.optics].

[36] N. M. Kroll, J. Appl. Phys. **36**, 34 (1965).

[37] Y. R. Shen and N. Blombergen, Phys. Rev. **137**, A1787 (1965).

[38] B. A. Auld, *Acoustic Fields and Waves in Solids* (Krieger, Malabar, 1990).

[39] L. D. Landau, L. P. Pitaevskii, and E. M. Lifshitz, *Course on Theoretical Physics* (Elsevier, New York, 2004).

[40] K. F. Graff, *Wave Motion in Elastic Solids* (Clarendon, Oxford, 1975).

[41] M. J. Ablowitz and H. Segur, *Solitons and the Inverse Scattering Transform* (SIAM, Philadelphia, 1981).

[42] D. F. Walls and G. J. Milburn, *Quantum Optics* (Springer, Berlin, 2008).

[43] M. Eichenfield, J. Chan, A. H. Safavi-Naeini, K. J. Vahala, and O. Painter, Opt. Express **17**, 20078 (2009).

[44] J. Chan, A. H. Safavi-Naeini, J. T. Hill, S. Meenehan, and O. Painter, Appl. Phys. Lett. **101**, 081115 (2012).

[45] N. R. Hill, Phys. Rev. B **24**, 7112 (1981).

[46] C. W. Gardiner and M. J. Collett, Phys. Rev. A **31**, 3761 (1985).

[47] W. Wustmann and V. Shumeiko, Phys. Rev. B **87**, 184501 (2013).

[48] A. Yariv, Yong Xu, R. K. Lee, and A. Scherer, Opt. Lett. **24**, 711 (1999).

[49] S. Datta, *Surface Acoustic Wave Devices* (Prentice-Hall, Englewood Cliffs, NJ, 1986).